Please cite this article in press as: Gee et al., Imaging Activity in Neurons and Glia with a *Polr2a*-Based and Cre-Dependent GCaMP5G-IRES-tdTomato Reporter Mouse, Neuron (2014), http://dx.doi.org/10.1016/j.neuron.2014.07.024

Neuron
NeuroResource

Imaging Activity in Neurons and Glia with a *Polr2a*-Based and Cre-Dependent GCaMP5G-IRES-tdTomato Reporter Mouse

J. Michael Gee,[1,5,6] Nathan A. Smith,[1,4,5] Fernando R. Fernandez,[1,5] Michael N. Economo,[3,5] Daniela Brunert,[3,5] Markus Rothermel,[3,5] S. Craig Morris,[1] Amy Talbot,[2] Sierra Palumbos,[2] Jennifer M. Ichida,[3] Jason D. Shepherd,[3] Peter J. West,[4] Matt Wachowiak,[3,5] Mario R. Capecchi,[2,7] Karen S. Wilcox,[4] John A. White,[1,5,*] and Petr Tvrdik[2,*]
[1]Department of Bioengineering
[2]Department of Human Genetics
[3]Department of Neurobiology and Anatomy
[4]Department of Pharmacology and Toxicology
[5]Brain Institute
[6]MD-PhD Program
[7]Howard Hughes Medical Institute
University of Utah, Salt Lake City, UT 84112
*Correspondence: john.white@utah.edu (J.A.W.), petr.tvrdik@genetics.utah.edu (P.T.)
http://dx.doi.org/10.1016/j.neuron.2014.07.024

SUMMARY

New strategies for introducing genetically encoded activity indicators into animal models facilitate the investigation of nervous system function. We have developed the PC::G5-tdT mouse line that expresses the GCaMP5G calcium indicator in a Cre-dependent fashion. Instead of targeting the *ROSA26* locus, we inserted the reporter cassette nearby the ubiquitously expressed *Polr2a* gene without disrupting locus integrity. The indicator was tagged with IRES-tdTomato to aid detection of positive cells. This reporter system is effective in a wide range of developmental and cellular contexts. We recorded spontaneous cortical calcium waves in intact awake newborns and evaluated concentration-dependent responses to odorants in the adult olfactory bulb. Moreover, PC::G5-tdT effectively reports intracellular calcium dynamics in somas and fine processes of astrocytes and microglial cells. Through electrophysiological and behavioral analyses, we determined that GCaMP5G expression had no major impact on nervous system performance. PC::G5-tdT will be instrumental for a variety of brain mapping experiments.

INTRODUCTION

Direct imaging of circuit activity in the live brain, from the network level down to subcellular resolution, is one of the most important recent innovations in neuroscience research. In particular, genetically encoded calcium indicators (GECIs) have enabled recording of activity in specific cell populations including both neurons and glia. The GFP-derived GCaMP family has become the most popular GECI (Nakai et al., 2001; Tian et al., 2009; Wachowiak et al., 2013). New and improved iterations of GCaMP have been developed including the GCaMP5 and GCaMP6 families (Akerboom et al., 2012; Chen et al., 2013). GCaMP5G is derived from semirandom mutagenesis of GCaMP3 and displays a higher signal-to-noise ratio (SNR) and a higher $\Delta F/F_0$ range, and it is superior to GCaMP3 for recording calcium transients in glial cells (Akerboom et al., 2012). GCaMP reporters permit tracking the activity of large assemblies of neurons and glia in awake and behaving animals, a technological breakthrough that is already stimulating progress in many areas of brain research (Brancaccio et al., 2013; Cui et al., 2013; Wachowiak et al., 2013; Yonehara et al., 2013).

The mouse is the preferred model for efficient implementation of genetically encoded neural activity indicators because of its readily modifiable genome and functionally complex nervous system. Transgenic lines with *Thy1* promoters have been instrumental for strong and selective expression of GCaMPs, demonstrating that noninvasive genetic approaches provide adequate signal and good viability of labeled cells (Chen et al., 2012). In comparison, Cre/lox and other site-specific recombination technologies offer optimized delivery of genetically encoded tools, enabling robust expression in a specific and reproducible manner. Recently, the Cre-dependent GCaMP3 reporter (Ai38) line was developed (Zariwala et al., 2012), demonstrating the advantages of this flexible genetic strategy. However, this reporter utilizes the common approach of targeting and disrupting the *ROSA26* locus, which in our experience reduces fecundity of homozygotes in certain genetic backgrounds and does not support high expression in cortical microglia.

To enable experiments in a wide array of cell types and systems, we have generated a Cre-dependent GCaMP5G line, termed PC::G5-tdT (*Polr2a*, CAG, GCaMP5G, tdTomato), with significant functional enhancements over previously generated GECI reporter mice. A separate fluorescent tag, tdTomato, is included in the design of the reporter cassette in order to aid the identification of cells with low intracellular calcium levels.

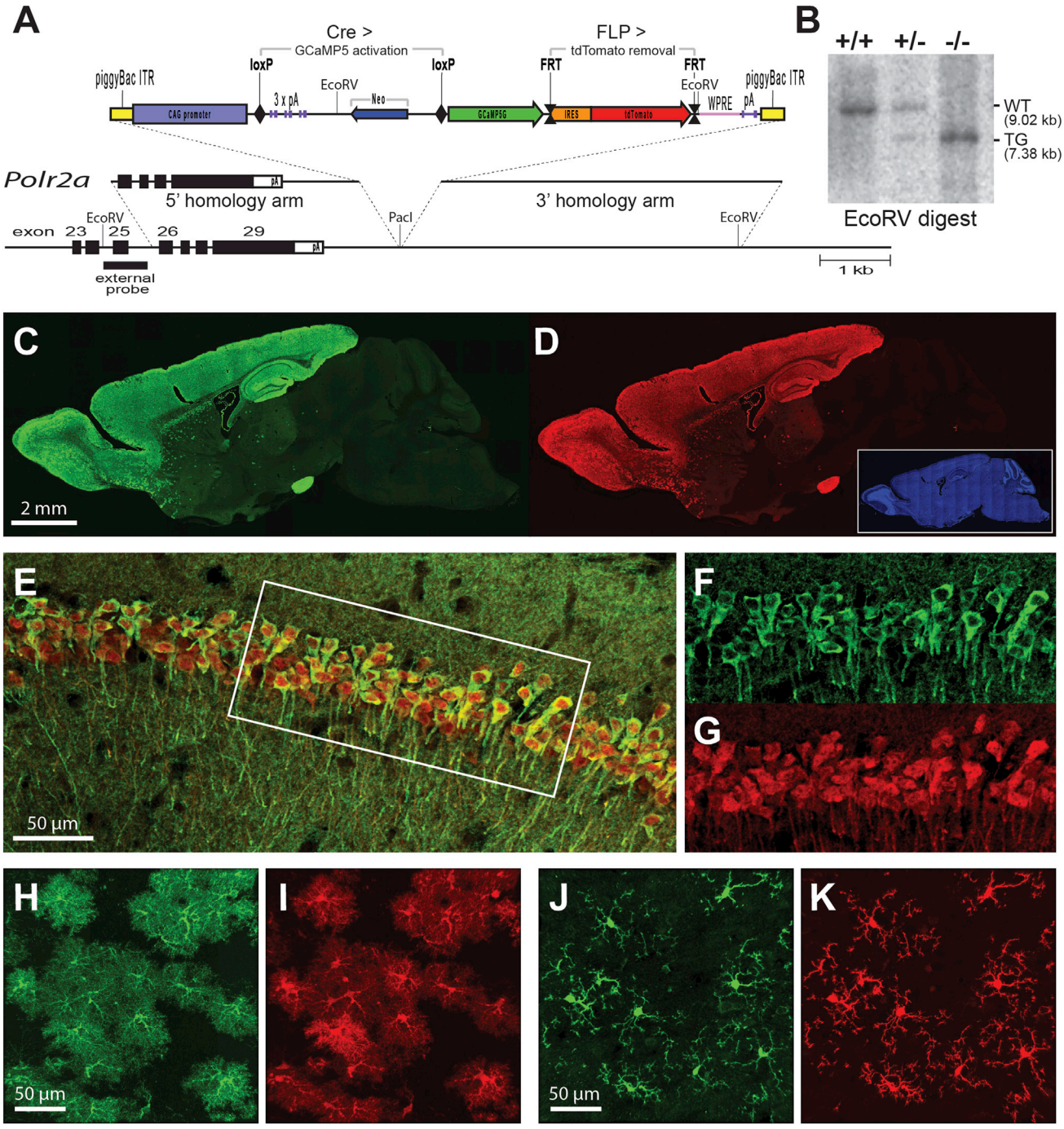

Figure 1. Generation and Characterization PC::G5-tdT

(A) A schematic diagram of the PC::G5-tdT allele. Both 5′ and 3′ homologies of the targeting vector are shown in relation to the endogenous *Polr2a* gene encoding the largest subunit of RNA polymerase II. The reporter component of the targeting vector is shown on top. The CAG promoter drives GCaMP5G and IRES-tdTomato expression following Cre-mediated excision of the STOP (3× pA) cassette. The IRES-tdTomato reporter can be independently removed with FLP recombinase. ITR, inverted terminal repeats; pA, polyadenylation signal; WPRE, woodchuck hepatitis posttranscriptional regulatory element.

(B) Southern blot analysis of tail DNA from control (+/+), heterozygous (+/−), and homozygous (−/−) *Polr2a*$^{CAG\text{-}GCaMP5G,tdTomato/CAG\text{-}GCaMP5G,tdTomato}$ animals. DNA was digested with EcoRV and hybridized with the external probe indicated in (A).

(C and D) Sagittal sections from heterozygous *Emx1-IRES-Cre*; PC::G5-tdT brains were stained with anti-GFP (GCaMP5G) and anti-RFP (tdTomato) antibodies and specifically imaged (C) in the green channel for GCaMP5G and (D) in the red channel for tdTomato. Blue DAPI staining is shown as an inset in (D).

(E–G) Hippocampal CA1 region of *CamKIIα-Cre*; PC::G5-tdT heterozygous animals stained with GFP and RFP antibodies. (E) Overlay of GCaMP5G and tdTomato signals. (F and G) Details of GCaMP5G and tdTomato signals, respectively, corresponding to the area framed with the white box in (E).

(legend continued on next page)

Importantly, by targeting the construct to the intergenic region 3′ of the ubiquitously expressed *Polr2a* gene, we maintain the transcriptional integrity of the mouse genome and enable genetic interaction with other tools inserted into the *ROSA26* locus without any linkage issues. In addition to displaying robust calcium responsiveness in various neuronal subtypes, the PC::G5-tdT reporter is highly active in the cell bodies and fine processes of both astrocytes and microglia in acute brain slices and in vivo. These features make the PC::G5-tdT line a powerful and flexible tool for the study of neuronal and glial networks in the mouse nervous system.

RESULTS

Generation and Characterization of the PC::G5-tdT Reporter Allele

The genetic strategy for the Cre-dependent GCaMP5G reporter mouse is presented in Figure 1A. The cytomegalovirus early enhancer and chicken beta actin (CAG) promoter and woodchuck hepatitis posttranscriptional regulatory element (WPRE) are utilized to facilitate high expression levels (Madisen et al., 2010; Zariwala et al., 2012). The cassette has been inserted in an intergenic region located 3′ of the gene for the largest subunit of RNA polymerase II (*Polr2a*; Figure 1B) and is flanked by inverted terminal repeats (ITRs) of piggyBac transposase. In the absence of Cre, transcription is prematurely terminated within the loxP-flanked RNA cleavage and polyadenylation module. After Cre recombination, both GCaMP5G and tdTomato become expressed in a bicistronic fashion. Because the internal ribosomal entry site (IRES)-tdTomato cassette is selectively flanked with FRT sites, it can be excised by FLP recombinase. If desired, a separate mouse line excluding tdTomato can thus be generated by breeding to the FLPe deleter (Rodríguez et al., 2000). We have termed the bicistronic line PC::G5-tdT (*Polr2a*, CAG, GCaMP5G, tdTomato). These mice breed well as homozygotes and can be obtained from JAX Mice (*Polr2a*$^{CAG\text{-}GCaMP5G,tdTomato}$, stock no. 024477).

To validate PC::G5-tdT, the reporter was crossed to *Emx1-IRES-Cre* (Gorski et al., 2002), *CaMKIIα-Cre* (Tsien et al., 1996), *Cck-IRES-Cre* (Taniguchi et al., 2011), *GFAP-CreER* (Chow et al., 2008), and *Hoxb8-IRES-Cre* (Chen et al., 2010) drivers. Consistent with previously reported expression patterns, the *Emx1-IRES-Cre* driver activates the reporter highly and in specific cell populations within the neocortex and olfactory bulb (Figures 1C and 1D), the *CaMKIIα-Cre* lineage is expressed strongly in the dentate gyrus and CA1 region of the hippocampus (Figures 1E–1G), and *GFAP-CreER* and *Hoxb8-IRES-Cre* direct expression to astrocytes and microglia, respectively (Figures 1H–1K). We also show that site- and cell-type specific and consistent induction of the sizeable GCaMP5G-IRES-tdTomato reporter can be achieved using Cre delivery based on adeno-associated virus (Figure S1 available online). Thus, GCaMP5G and tdTomato can be expressed strongly in a variety of specific cell types. Intracellular distribution of both markers varies slightly, despite the similar size of their polypeptide chains. While tdTomato is distributed evenly throughout most of the nucleus and cytosol, GCaMP5G is excluded from the nucleus in normal healthy cells (Figures 1F and 1G).

To verify that the CAG promoter targeted adjacent to the *Polr2a* gene is expressed ubiquitously and consistently in various tissues and developmental stages, PC::G5-tdT was crossed to *HPRT-Cre* deleter mice (Tang et al., 2002) to activate the reporter in all cells. We then evaluated the expression of GCaMP5G and tdTomato proteins with immunohistochemistry in embryonic day E14.5 sections and in sagittal sections of postnatal day 1 (P1) heads and in adult brains (Figures S2 and S3). Our data indicate that although both markers exhibit somewhat lower expression in visceral organs, such as fetal liver, CAG expression in the nervous system is consistently high throughout development. Thus, PC::G5-tdT is a useful genetic platform for expressing genetic tools in neurons and glia.

Next we asked if high expression levels of GCaMP5G impact normal physiology and behavior in this model. To limit the effects to the GCaMP5G protein alone, PC::G5-tdT was crossed to a FLPe deleter mouse (Rodríguez et al., 2000) in order to remove the tdTomato tag (PC::G5) and subsequently to a *HPRT-Cre* deleter (Tang et al., 2002) to turn on GCaMP5G expression in the germline and consequently in all cells of the body. Three heterozygous male founders were crossed with C57Bl/6 females and the offspring segregated normally (11 GCaMP5G positive animals, 10 negative controls). The groups did not differ in body weight at 2 months of age (23.2 ± 1.15 g and 23.6 ± 1.89 g for GCaMP5G and control males, respectively, and 18.4 ± 1.11 g and 18.3 ± 1.05 g for GCaMP5G and control females, respectively [numbers are means ± SD]; no body weight differences were observed later in life either). This cohort was subjected to behavioral testing.

Analysis of spontaneous home cage behavior with the automated behavioral platform Laboras (Chen et al., 2010) revealed no significant differences in any of the classified behavioral categories (Figures S4A–S4G). Both groups spent a comparable amount of active time in locomotor behavior, rearing, and climbing and traveled a similar distance over the span of 24 hr (Figures S4A–S4D). Eating, grooming, and sleeping or immobility were also unchanged (Figures S4E–S4G). Potential ambulatory deficits measured with Rotarod confirmed that GCaMP5G mice have normal motor coordination (Figure S4H). The prepulse inhibition (PPI) test with acoustic stimuli is an accurate neurological assessment of the brain circuits involved in rapid information processing, and disruptions of PPI are well documented in mouse models of schizophrenia and other mental disorders (Powell et al., 2009). To test if these circuits function normally in the GCaMP5G animals, PPI experiments were performed with the SR-LAB startle reflex system. At all prepulse levels (+3, +6, and +12 dB above background), the mean values of PPI in GCaMP5G mice did not significantly differ from controls

(H–K) Cortical astrocytes from *GFAP-CreER*; PC::G5-tdT animals (H and I) and cortical microglia from brains of *Hoxb8-IRES-Cre*; PC::G5-tdT genotype (J and K). Both astrocytes and microglia were stained as above and specifically imaged (H and J) for GCamP5G and (I and K) for tdTomato. Adult animals ranging in age from 5 to 8 weeks were used for immunohistochemistry in (C)–(K).
See also Figures S1–S4.

(Figures S4I–S4K). Together, these experiments demonstrate that GCaMP5G-expressing mice display no substantial anatomical or behavioral deficits and this model is therefore suited for complex experiments involving neurophysiology, imaging, and behavior.

Spontaneous Cortical Waves in Intact Neonates

Many Cre-dependent fluorescent protein-labeled cell lineages can be detected in live mouse newborns with epifluorescence equipment. Due to the inclusion of the bright tdTomato marker in PC::G5-tdT, it is possible to visualize desired expression patterns with handheld fluorescence devices, such as the NIGHTSEA BlueStar Flashlight. For example, in crosses with the previously mentioned *Emx1-IRES-Cre* line, tdTomato-labeled cells are seen in the cerebral cortex and limbs (Figure 2A). The benefit is 2-fold. First, this feature allows identification of required allelic combinations in offspring without genotyping, saving time and cost. Second, visual inspection of the gene expression patterns enables the researcher to distinguish specific cell lineages from generalized recombination commonly occurring in the germline of certain Cre drivers or aging animals. The latter advantage is of high significance as it precludes acquisition of confounding experimental data from nonspecific genetic models.

Serendipitously, when observing *Emx1-IRES-Cre*; PC::G5-tdT under a fluorescence stereoscope with GFP filters, we noted that cortical waves of neural activity can be viewed through the eyepiece in intact newborns. To analyze this phenomenon further, a wide-field epifluorescence microscope equipped with a fast CCD camera was employed to image spontaneous calcium waves in the cortex of awake and gently restrained P2 pups (Figures 2B–2H; Movie S1). We measured cortical activity through intact skin and bone for three 60 s trials per animal (n = 4) and analyzed a total of 161 events. Changes in GCaMP5G fluorescence were readily detectable ($\Delta F/F_0 > 40\%$). Spontaneous activity was frequent in putative primary visual cortex (V1; 11.87 events/min), auditory cortex (A1; 3.39 events/min), and primary somatosensory cortex (S1; 5.74 events/min). Large, synchronous activity waves were observed in the limb regions of S1 (Figure 2C). Quantitative traces integrating the regions of interest reveal the presence of both unilateral (primarily in the visual cortex) and synchronous bilateral (limb somatosensory) spontaneous events (Figure 2I). Little or no activity was observed in more rostral motor cortex areas. We detected significant intraregional differences in mean intensity peak $\Delta F/F_0$ (A1: 5.6 ± 4.8; S1: 9.8 ± 6.9; V1: 5.0 ± 4.7; Figure 2J), but not duration (A1: 3.9 ± 1.5; S1: 4.1 ± 1.9; V1: 4.4 ± 2.0 s; Figure 2K) or mean event diameter (A1: 590 ± 61.1; S1: 514 ± 135.5 μm; V1: 547.4 ± 104.2 μm; Figure 2L). The mean velocity of cortical calcium wave propagation was 3.6 ± 2.9 mm/s (ranging from 0.3 to 13.1 mm/s), consistent with previously reported values (Namiki et al., 2013). There were no significant differences detected in wave velocity between cortical regions ($p = 0.22$, one-way ANOVA). Numbers are means ± SD.

Spontaneous early network oscillations during neonatal development of the CNS are involved in facilitating the proper patterning of activity in the postnatal brain (Adelsberger et al., 2005). Here we show that these phenomena can be studied in intact and behaving neonates during early postnatal life with the PC::G5-tdT reporter. The lineage-specific nature of this technique will permit dissecting individual neuronal and glial cell types during this stage of brain development.

Evoked Calcium Transients in the Olfactory Bulb

In order to determine the performance of GCaMP5G in specific neural circuits of the adult mouse brain, we crossed PC::G5-tdT with *Emx1-IRES-Cre* and *Cck-IRES-Cre* drivers, which target expression to olfactory bulb excitatory neurons (mitral and tufted cells) with dendritic projections to glomeruli (Gorski et al., 2002; Seroogy et al., 1985). We imaged odorant-evoked glomerular activity on a two-photon microscope through a cranial window implanted over the dorsal surface of the olfactory bulb. Different odorants were delivered directly to the olfactory epithelium with high temporal precision via a computer-controlled flow-dilution olfactometer and an artificial inhalation scheme (Wachowiak et al., 2013). tdTomato fluorescence remained stable throughout the recordings with minimal photobleaching (Figures 3C and 3F), and robust and reproducible glomerular calcium transients were observed (Figures 3A, 3B, 3D, and 3E). Different odorants evoked distinct patterns of glomerular activation, with peak fluorescence increases of greater than 200% (Figures 3A–3F). Higher-magnification imaging revealed strong GCaMP5G fluorescence increases in mitral and tufted cell dendritic tufts within glomeruli and also in their primary and lateral dendrites (Figures 3J and 3L). Increasing odorant concentrations recruited activation of additional glomeruli and led to an increase in signal amplitude (Figures 3G–3K), consistent with response characteristics reported previously using virally expressed GCaMP5G or GCaMP3 reporter expression (Kato et al., 2012; Wachowiak et al., 2013). In four mice we compared odorant-evoked fluorescence signals imaged from the glomerular dendritic tufts of *Cck*-positive neurons expressing either GCaMP5G or GCaMP3 using the *Cck-IRES-Cre* driver line crossed with PC::G5-tdT (two mice) or the Ai38 *ROSA26*-GCaMP3 reporter (two mice; Zariwala et al., 2012). Peak GCaMP signals evoked by the same odorant (1% ethyl butyrate) across glomeruli located in the same region of the dorsal olfactory bulb were substantially larger for the GCaMP5G reporter than for the GCaMP3 reporter (Ai38: 38.8% ± 12.4% $\Delta F/F_0$ [n = 10 glomeruli]; PC::G5-tdT: 110.3% ± 38.1% $\Delta F/F_0$ [n = 8 glomeruli]; $p < 0.0001$; unpaired two-tailed t test, numbers are means ± SD). Overall, these results establish the PC::G5-tdT line as an effective tool for imaging activity in genetically defined neural circuits in vivo and are consistent with the improvements in optical signal size over GCaMP3 that have been previously demonstrated with viral expression.

Characterization of Spike-Evoked Calcium Signals in CA1 Pyramidal Neurons

To characterize the sensitivity and signaling properties of the PC::G5-tdT reporter in individual neurons, we performed whole-cell recordings from hippocampal CA1 pyramidal neurons in acute brain slices from *CaMKIIα-Cre*; PC::G5-tdT animals. Identification of Cre-positive cells targeted for electrophysiological recordings and calcium imaging was greatly facilitated when tdTomato fluorescence was employed for guidance. Figure 4A

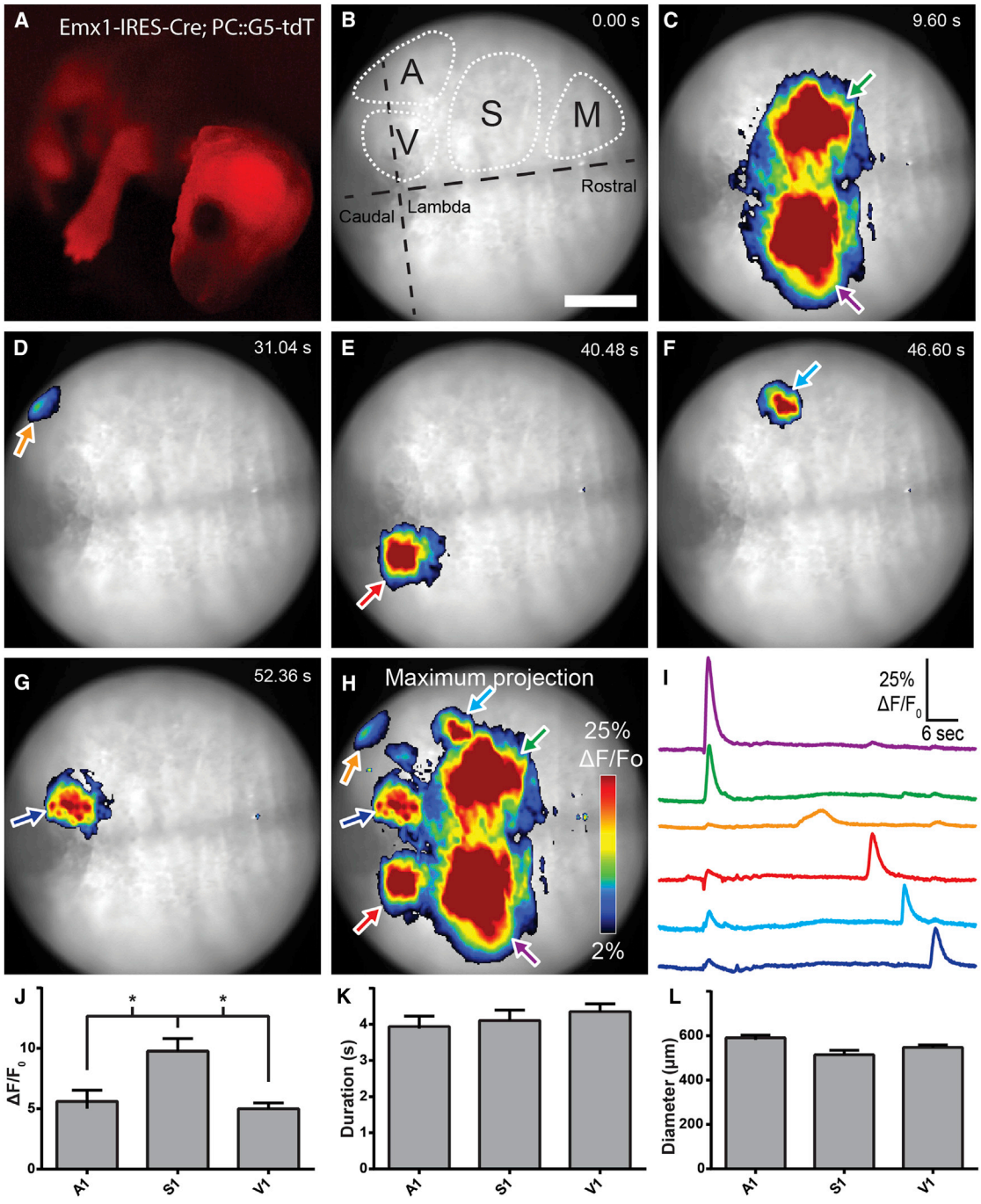

Figure 2. Recording Spontaneous Calcium Activity in Intact, Awake, and Behaving Neonates

(A) tdTomato expression in *Emx1-IRES-Cre*; PC::G5-tdT.

(B–G) Frames from a movie demonstrating spontaneous transients throughout the cortex. Scale bar, 1 mm. (B) Putative cortical areas are indicated. A, auditory cortex; M, motor cortex; S, somatosensory cortex; V, visual cortex (Joshi et al., 2008).

(H) Maximum projection of activity from the movie used for (B)–(G).

(I) $\Delta F/F_0$ traces corresponding to regions of interest in (H). The line colors correspond to the arrow outline colors in (H).

(J) Peak of $\Delta F/F_0$ events by putative cortical region.

(K) Duration of events.

(L) Diameter of events. P2 pups were used for experiments.

Bar graphs display means ± SEM. See also Movie S1.

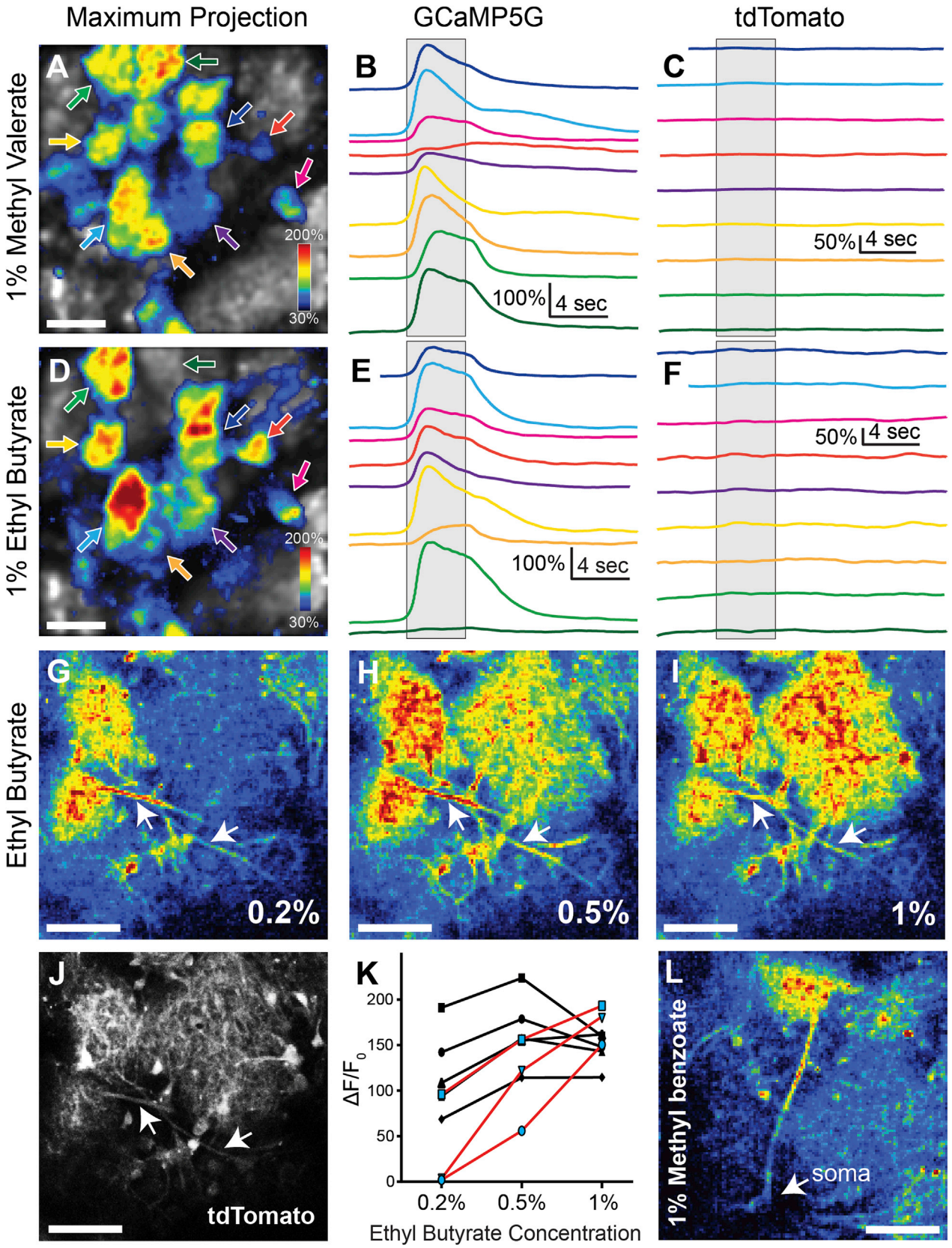

(legend on next page)

shows a full raster scan image of tdTomato fluorescence in CA1 pyramidal neurons and examples of GCaMP5G fluorescence during current-evoked spiking. Although we only evaluated current-evoked fluorescence in hippocampal slices, we have also imaged cortical neurons in vivo and both *CaMKIIα*- and *Cck*-positive neurons were readily detected in layer 2/3 of the barrel cortex (Figure S5).

To precisely quantify calcium events in patched neurons, we used fast line scan imaging across neuronal cell bodies during different levels of current-evoked depolarization and spike count generation (Figure 4B). Pyramidal cells were depolarized gradually using current steps of increasing size that elicited a range of spike frequencies (Figures 4B and 4C; Movie S2). For the spike firing range of CA1 pyramidal cells (0–40 spikes/s), the relationship between peak fluorescence and spike count was approximately linear (r^2 = 0.93, n = 18 cells), with a change in peak $\Delta F/F_0$ of 6.5% ± 0.7% per each additional spike elicited (Figure 4D). Detectable fluorescence responses were observed at a minimum of two spikes, which resulted in a significant change in the mean peak $\Delta F/F_0$ (Figure 4D; $\Delta F/F_0$ = 14.1% ± 4.5%, p = 0.01, n = 9 cells). For the same data set we also calculated the peak SNR. Peak SNR values ranged from 3.3 ± 0.8 at 1 spike to 24.1 ± 5.6 at 17 spikes (Figure S6A).

To quantify the response kinetics of GCaMP5G in this reporter, we used independent exponential fits for the rise and decay time of the fluorescence signal response elicited during 5, 10, and 15 spikes. For fits, we used signals that elicited a minimum $\Delta F/F_0$ of 10%. The rising phase of the fluorescence response was fit with a single exponential function raised to the power of four, while the decay time course was fit using a standard single exponential decay function (Figure 4E). Mean rise time constants were significantly smaller than decay time constants (Figure 4F; $p < 0.001$, two-way ANOVA). However, the rise and decay kinetics did not depend on the number of spikes underlying the fluorescence response (Figure 4F; p = 0.44, two-way ANOVA).

GCaMP5G protein displays a relatively high calcium binding affinity with K_d = 460 ± 11 nM (Akerboom et al., 2012), and the possibility of interference due to buffering of intracellular calcium levels is a concern. To further investigate if hippocampal neuronal intrinsic properties and synaptic plasticity are affected by this interference, we performed experiments in acute brain slices from the *CaMKIIα-Cre*; PC::G5-tdT animals to evaluate both frequency-current (*f-I*) relationships and long-term potentiation (LTP) at the Schaffer collateral synapses between CA3 and CA1 pyramidal neurons. For *f-I* relationships, neither rheobase (minimum current required to elicit spiking) nor gain (slope of *f-I* relationship) were significantly changed in PC::G5-tdT animals (Figures S6B and S6C), although the maximum firing rate tended to be somewhat higher (Figures S6D and S6E). Synaptic plasticity, as assessed by posttetanic and LTP following theta burst stimulation as previously described (West et al., 2014), were unchanged (Figure S7). Therefore, at least in heterozygous PC::G5-tdT animals, expression of the GCaMP5G calcium indicator does not alter single-cell electrophysiological properties or synaptic plasticity within the CA3-CA1 circuit. Our findings are consistent with results from similar experiments examining electrophysiological properties of GCaMP3-expressing astrocytes (Haustein et al., 2014; Shigetomi et al., 2013).

Monitoring Spontaneous and Evoked Calcium Dynamics in Astrocyte Somas and Processes

Astrocytes play a prominent role in the maintenance and modulation of neural circuits (Anderson and Swanson, 2000; Ballabh et al., 2004; Haydon, 2001; Nedergaard et al., 2003; Wang et al., 2012), but experimental approaches available for studying their activity have been limited. In astrocytes, calcium imaging dependent on synthetic dye loading is technically very challenging in adult or pathological tissue. Even with successful dye loading in young healthy tissue, astrocyte processes are difficult to visualize because of problems with diffusion to cellular termini. While endogenously encoded indicators have proven to be superior to other imaging approaches in astrocytes (Shigetomi et al., 2013), effective transgenic reporters have been lacking.

We therefore tested the utility of the PC::G5-tdT line for the investigation of astrocytes by crossing with the tamoxifen-inducible *GFAP-CreER* line (Chow et al., 2008). Following a single tamoxifen injection (225 mg/kg intraperitoneally), numerous astrocytes throughout the brain were labeled by expression of both GCaMP5G and tdTomato (Figures 1H and 1I). tdTomato expression was beneficial for selection of astrocytes prior to calcium imaging (Figure 5A). In agreement with previous reports, a few neurons exhibited GCaMP5G signals due to *Gfap* expression in neuronal progenitors (Casper and McCarthy, 2006; Doetsch et al., 1999; Garcia et al., 2004; Laywell et al., 2000; Seri et al., 2001).

Figure 3. Odor-Evoked Neural Activity in the Olfactory Bulb

(A) Maximum projection of GCaMP5G $\Delta F/F_0$ in the olfactory bulb following 1% methyl valerate administration in a 2-month-old *Emx1-IRES-Cre*; PC::G5-tdT. Arrows specify individual glomeruli.

(B) Mean GCaMP5G $\Delta F/F_0$ traces from four trials. The line colors correspond to the arrow colors in (A). The gray box indicates the precise timing of odorant administration.

(C) Mean tdTomato $\Delta F/F_0$ traces.

(D–F) Same as (A)–(C) except with ethyl butyrate administration. Different odors in (A)–(C) and (D)–(F) elicited different patterns of glomeruli activity in the same region of interest.

(G) tdTomato expression of the region shown in (H)–(J). Arrowheads denote dendritic projections to glomeruli.

(H–J) GCaMP5G $\Delta F/F_0$ response at three different odor concentrations in a P125 *Cck-IRES-Cre*; PC::G5-tdT.

(K) Peak GCaMP5G $\Delta F/F_0$ from individual glomeruli at three concentrations of ethyl butyrate. Those displaying graded responses are shown in red.

(L) Mean peak $\Delta F/F_0$ response of glomeruli exhibiting graded responses in (K). A significant difference was detected between groups using a one-way ANOVA, and Tukey's post hoc test revealed a statistical difference between peak GCaMP5G $\Delta F/F_0$ in the 0.2% and 1% groups (p = 0.04).

(M) Intensity image of a single tufted cell projecting to a glomerulus in response to 1% methyl benzoate. In (A) and (D) the scale bar represents 100 μm, and in (G)–(J) and (L) the scale bar represents 50 μm. Bar graphs display means ± SEM.

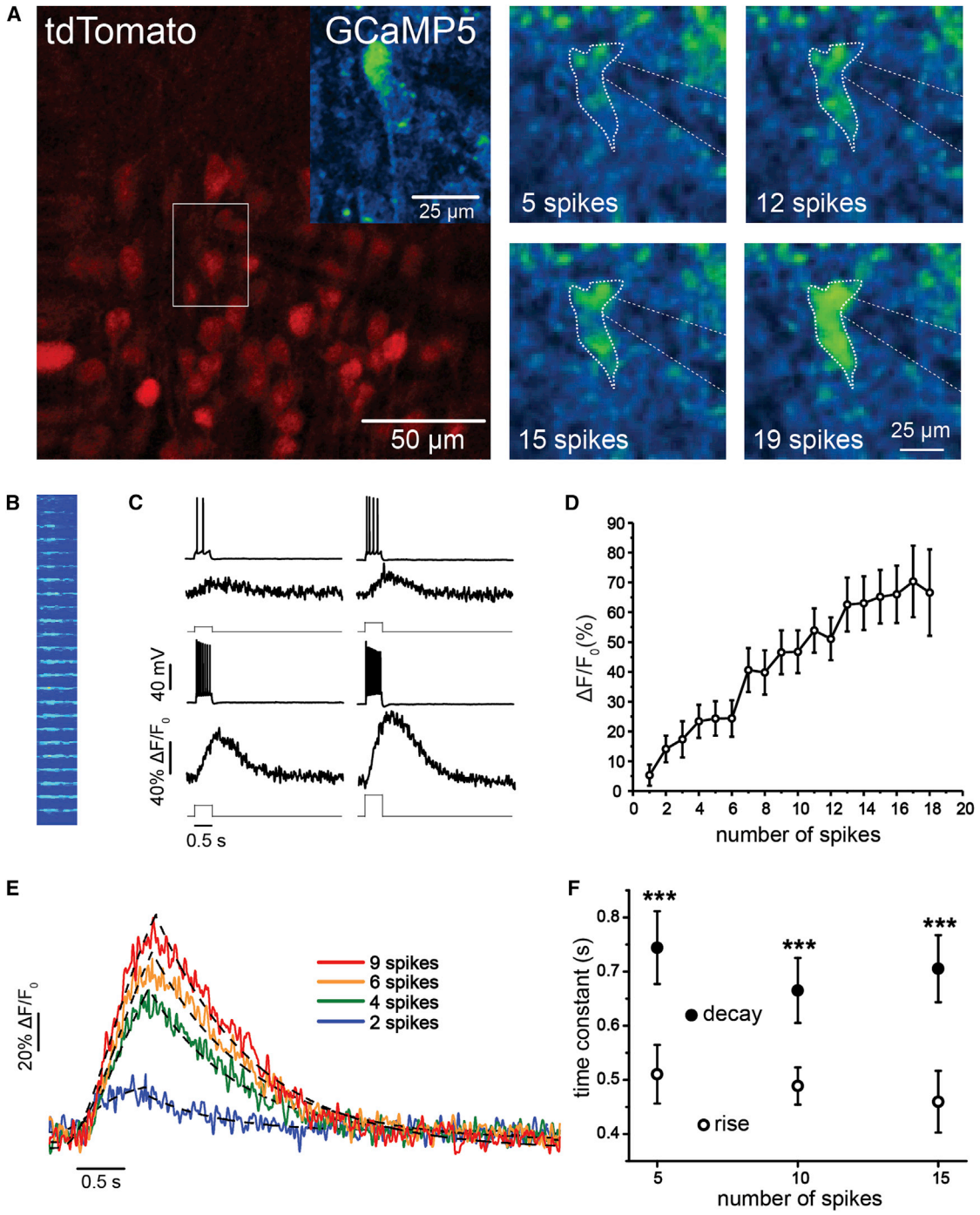

Figure 4. Quantification of Spike-Evoked GCaMP5G Fluorescence Signals in CA1 Pyramidal Cells

(A) A patched CA1 pyramidal cell expressing tdTomato and GCaMP5G (inset) in a *CaMKIIα-Cre*; PC::G5-tdT. The panels on the right demonstrate GCaMP5G fluorescence intensity changes in a single CA1 pyramidal cell during current-evoked spiking acquired using a full raster scan.

(B) Line scan image of GCaMP5G fluorescence resulting from increasing levels of current-evoked depolarization.

(C) Representative time series of membrane voltage and $\Delta F/F_0$ responses to current-evoked signals for four different current step sizes and spike count numbers.

(D) Plot of $\Delta F/F_0$ showing mean CA1 pyramidal cell population responses.

(E) Kinetics of GCaMP5G fluorescence signals. The rise and decay time course of individual $\Delta F/F_0$ signals elicited by different spike counts (colored lines) were fitted with exponential functions (dashed lines).

(F) Mean time constants associated with rise times were significantly shorter than those of decay times across a range of stimulus intensities and spike counts. Data are means ± SEM. ***$p < 0.001$ between rise and decay time constants. All experiments were performed on 4- to 8-week-old mice.

See also Figures S5–S7 and Movie S2.

Please cite this article in press as: Gee et al., Imaging Activity in Neurons and Glia with a *Polr2a*-Based and Cre-Dependent GCaMP5G-IRES-tdTomato Reporter Mouse, Neuron (2014), http://dx.doi.org/10.1016/j.neuron.2014.07.024

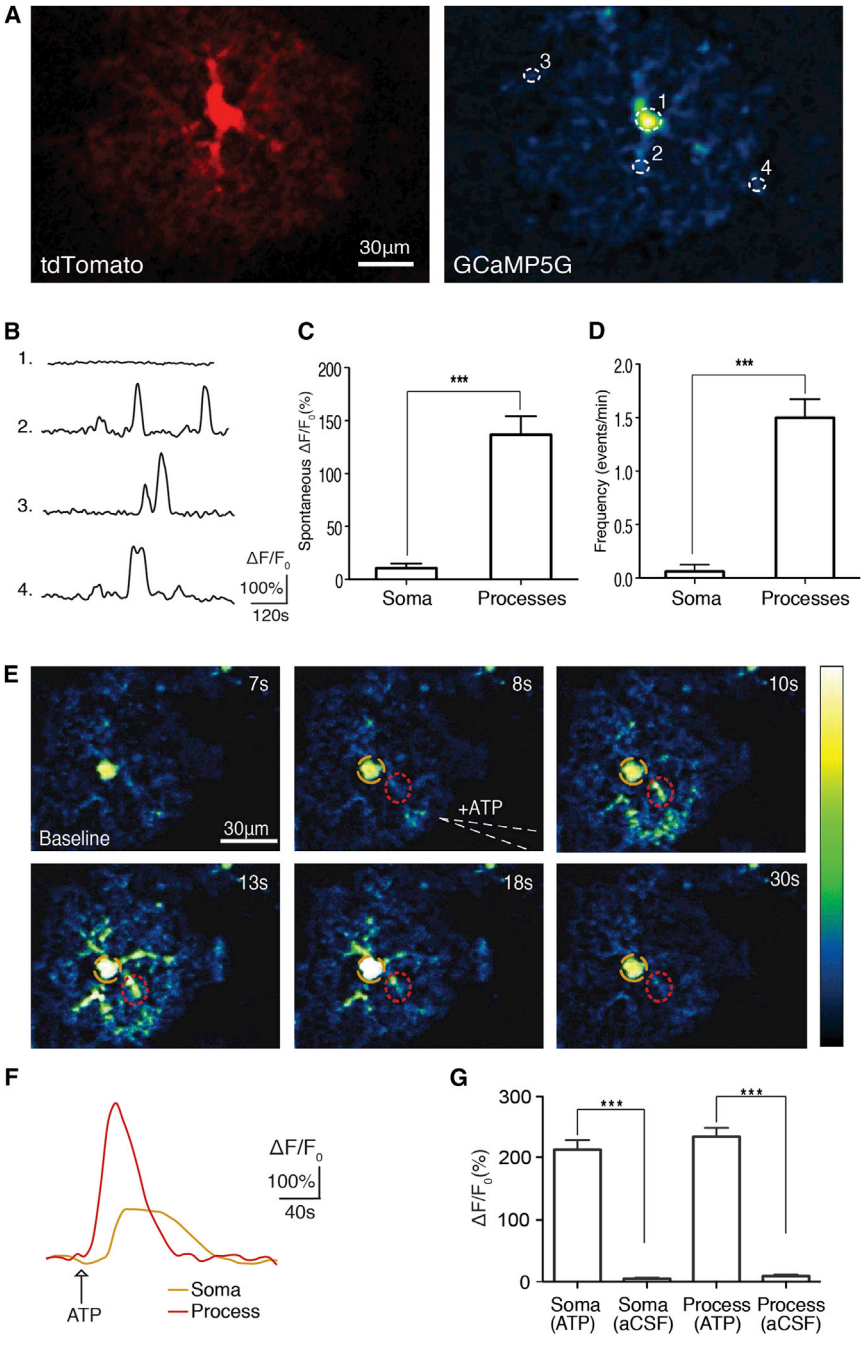

Figure 5. Spontaneous and Evoked Calcium Dynamics in Astrocytes In Vitro

(A) A cortical astrocyte expressing tdTomato and GCaMP5G.

(B) Representative individual traces of GCaMP5G fluorescence changes ($\Delta F/F_0$) in spontaneous astrocyte activity. White dotted circles in (A) correspond to ROIs in the soma and processes.

(C) Histogram comparing the mean spontaneous calcium $\Delta F/F_0$ in somas and processes (***$p < 0.0003$; unpaired t test; n = 8–24 cells).

(D) Histogram comparing the mean frequency of spontaneous calcium transients in astrocyte somas and processes (***$p < 0.0001$; unpaired t test; n = 8–24 cells).

(E) Time series of intracellular calcium increases induced by focal application of ATP (100 μM) from a glass pipette (white dotted line) in an acute brain slice prepared from a *GFAP-CreER*; PC::G5-tdT. The pseudocolor scale displays relative changes in GCaMP5G emission intensity.

(F) Representative individual traces of GCaMP5G fluorescence changes ($\Delta F/F_0$) in response to ATP administration. The color-coding of the traces matches the colored circles in (E).

(G) Histogram comparing the mean ATP induced calcium increases in somas and processes of astrocytes (***$p < 0.0001$; paired and unpaired t test before and after ATP or vehicle application; n = 8–19 cells). Experiments were performed on 4- to 8-week-old mice.

Bar graphs display means ± SEM. See also Movies S3 and S4.

To investigate the functionality of GCaMP5G in astrocytes, we used acute brain slices from 4- to 8-week-old mice. First, we assessed spontaneous calcium transients in cortical astrocyte somas and processes. We observed large localized calcium transients throughout astrocyte processes, but only small somatic events (Figure 5B; Movie S3). The mean spontaneous transient amplitude measured during 2 min recordings in processes was 136.7% ± 17.64% (n = 24 cells) and 10.6% ± 4.51% in somas (n = 8 cells; Figure 5C). As previously reported, calcium transients were detected throughout the entire astrocyte territory but were most frequent in processes within 10–50 μm of the soma (Movie S3; Shigetomi et al., 2013). The mean frequency of process transients was 1.5 ± 0.17 transients/min (n = 24 cells) and 0.06 ± 0.06 transients/min in somas (n = 8 cells; Figure 5D).

Next, we investigated direct activation of astrocytes by focal application of ATP, a P2Y agonist known to induce calcium release from internal stores. Focal ATP (100 μM) administration evoked a cytosolic calcium increase in both astrocyte processes and somas in cortex that propagated across the field of view as a wave (Figures 5E and 5F; Movie S4). The mean ATP-evoked peak $\Delta F/F_0$ in processes was 235.1% ± 14.21% (n = 19 cells) and in somas was 214.0% ± 15.62% (n = 19 cells; Figure 5G). Focal application of artificial cerebrospinal fluid (aCSF) (vehicle) did not evoke a significant calcium rise in astrocyte processes (9. 0% ± 2.74%, n = 8 cells) or somas (4.9% ± 1.64%, n = 8 cells; Figure 5G).

To further establish the ability of GCaMP5G to report calcium transients in astrocytes, we evaluated evoked calcium responses in vivo through sensory stimulation (Figure 6A). Previous studies have demonstrated that astrocytes in barrel cortex

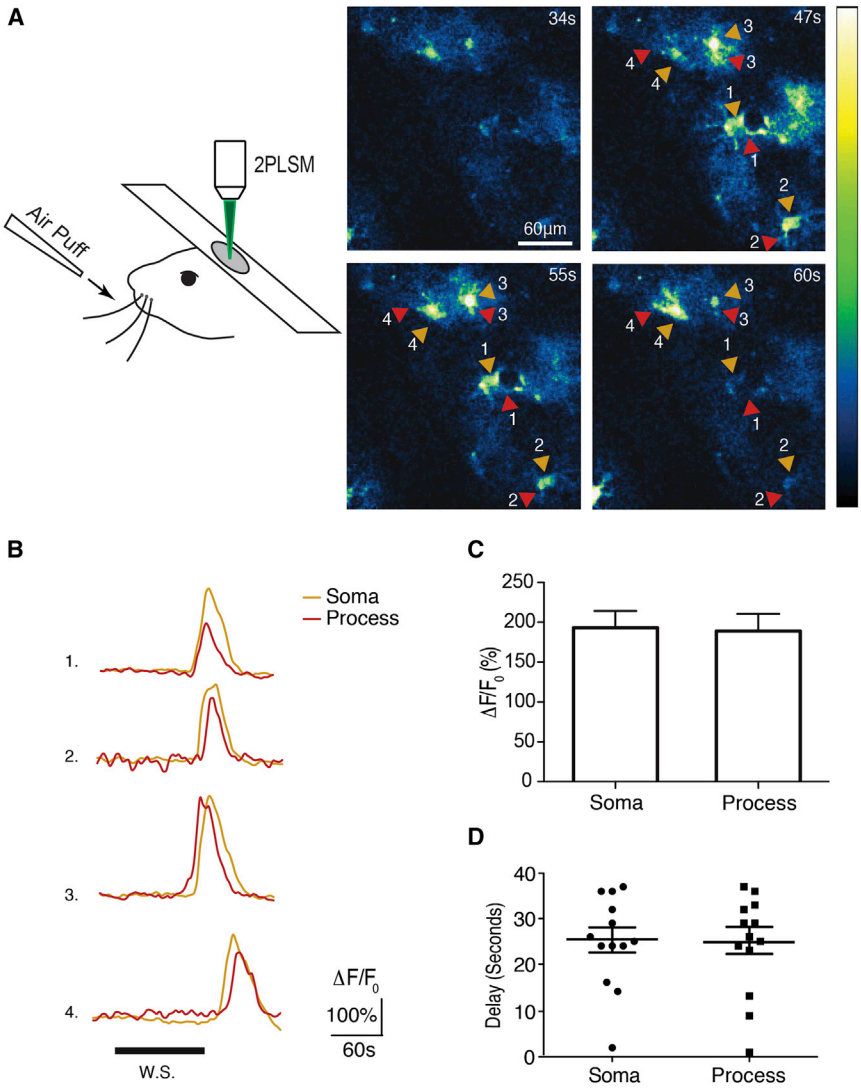

Figure 6. Evoked Calcium Dynamics in Astrocytes In Vivo

(A) Two-photon microscopy (2PLSM) used to image astrocyte calcium responses to 30 s of 5 Hz whisker stimulation in layer 2/3 of barrel cortex. (Right) Time series of whisker stimulation-evoked calcium increases in astrocytes located 100–150 μm below the pial surface. The pseudocolor scale displays changes in GCaMP5G $\Delta F/F_0$.

(B) Representative individual traces of GCaMP5G fluorescence changes ($\Delta F/F_0$) in response to whisker stimulation. Arrows correspond to astrocyte somas (orange) and processes (red).

(C) Histogram comparing the whisker stimulation-evoked $\Delta F/F_0$ in astrocyte somas and processes ($p = 0.85$; paired t test; $n = 3$ mice).

(D) Scatter plot comparing the mean delay between the onset of whisker stimulation and the emergence of GCaMP5G responses in astrocyte somas and processes ($p = 0.88$; paired t test; $n = 3$ mice). Experiments were performed on 5- to 8-week-old mice.

Bar graphs display means ± SEM. See also Movie S5.

respond to whisker stimulation with calcium increases in both lightly anesthetized and awake behaving animals (Ding et al., 2013; Thrane et al., 2012; Wang et al., 2006). Using a similar whisker stimulation protocol (5 Hz, 30 s) in anesthetized mice, we evoked large calcium transients in the somas and processes of astrocytes (Figures 6A and 6B; Movie S5). The mean whisker stimulation-evoked calcium increase in processes was 189% ± 21.30% and in somas was 193.1% ± 21.21% (Figure 6C). We also observed variable time delays in sensory evoked calcium responses following onset of whisker stimulation. The mean delay between the onset of whisker stimulation and the initial appearance of calcium responses was 24.4 ± 2.98 s in processes and 25.0 ± 2.76 s in somas (Figure 6D), in agreement with a previous study (Ding et al., 2013). It is worth noting that some sensory evoked calcium transients in our experiments may have been suppressed by anesthesia, as it has been shown that astrocytes exhibit reduced calcium signaling in the presence of anesthetics (Thrane et al., 2012). Together, these data provide evidence that PC::G5-tdT can effectively monitor spontaneous and evoked calcium dynamics in astrocytes in vitro and in vivo.

PC::G5-tdT Is a Sensitive Indicator of Calcium Transients in Microglia

Microglia, the resident immune cells of the central nervous system, have not been subjected to many rigorous intracellular calcium monitoring experiments due to substantial technical challenges (Brawek et al., 2014). In order to express GCaMP5G in microglia, we crossed PC::G5-tdT to the *Hoxb8-IRES-Cre* driver (Chen et al., 2010). Expression levels in microglial cells were high (Figures 1J and 1K). However, when we imaged acute brain slices with two-photon microscopy, spontaneous calcium transient were negligibly rare, consistent with previous reports (Eichhoff et al., 2011).

Microglia also express several purinergic receptors, primarily metabotropic subtypes such as P2RY12, P2RY13, and P2RY6 (Hickman et al., 2013). To evaluate calcium responses in microglia via purinergic receptor stimulation, we focally applied ATP (100 μM). Similar to what was observed in astrocytes, ATP evoked a significant cytosolic calcium increase in both microglia processes and somas (Figures 7A and 7B; Movie S6). The mean ATP-evoked peak $\Delta F/F_0$ in microglia processes was 91.0% ± 6.89% ($n = 7$) and in somas it was 81.0% ± 11.73% ($n = 7$) (Figure 7C). Focal application of aCSF (vehicle) did not elicit a significant calcium response in microglia processes (peak $\Delta F/F_0$ of 11.3% ± 3.90%, $n = 4$) or somas (peak $\Delta F/F_0$ of 8.3% ± 2.06%, $n = 4$) (Figure 7C). To test if we could further improve sensitivity by increasing the gene dosage of the GCaMP5G, we repeated the experiments with acute brain slices from

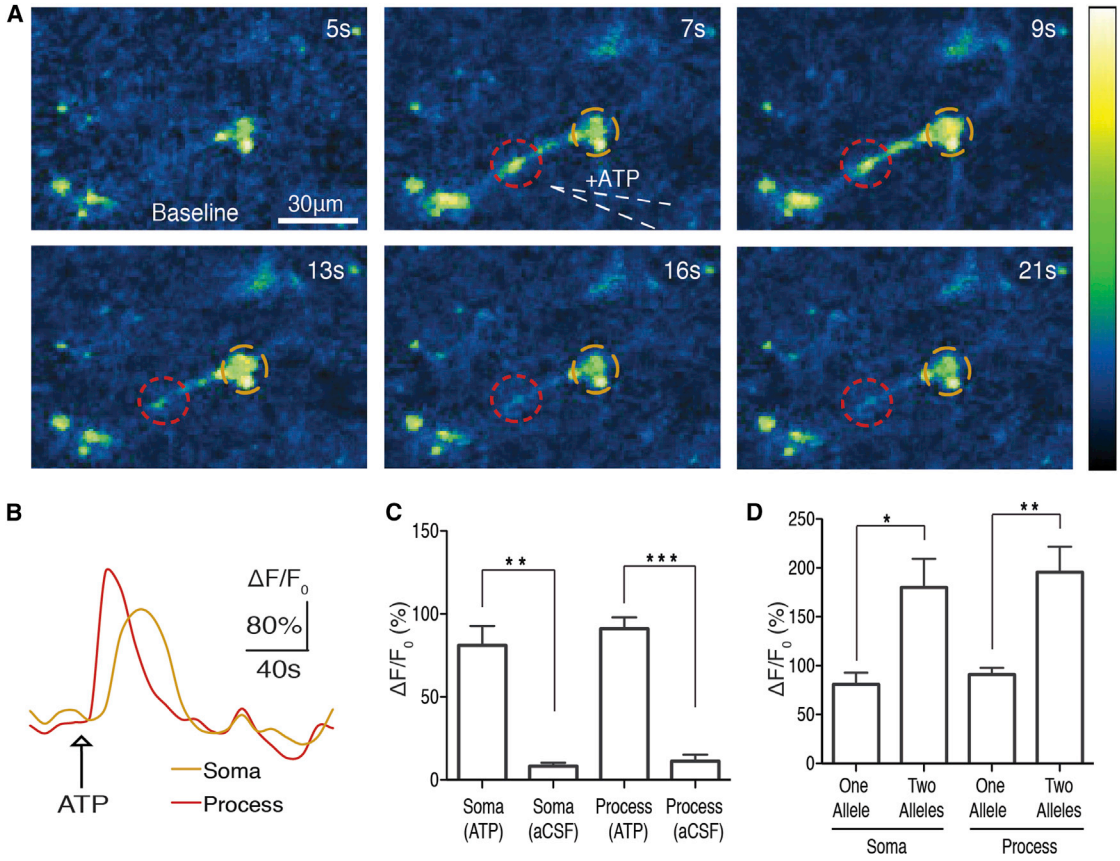

Figure 7. PC::G5-tdT Is a Sensitive Indicator of Calcium Transients in Microglia

(A) Time series of intracellular calcium increases induced by focal application of ATP (100 μM) from a glass pipette (white dotted line) in an acute brain slice prepared from a *Hoxb8-IRES-Cre*$^{+/-}$; PC::G5-tdT$^{+/-}$. The pseudocolor scale displays relative changes in GCaMP5G emission.

(B) Representative individual traces of GCaMP5G fluorescence changes ($\Delta F/F_0$) in response to ATP administration. The color-coding of the traces matches the colored circles in (A).

(C) Histogram comparing the mean ATP-induced calcium increases in somas and processes of microglia (**$p < 0.01$, ***$p < 0.0001$; paired and unpaired t test before and after ATP or vehicle application; n = 4–7 cells).

(D) Histogram comparing the mean ATP-induced peak $\Delta F/F_0$ in the somas and processes of microglia with a single allele (heterozygous) and two alleles (homozygous) of GCaMP5G (*$p < 0.05$, **$p < 0.01$; paired and unpaired t test before and after ATP application; n = 7–10 cells). All experiments were performed on 4- to 8-week-old mice.

Bar graphs display means ± SEM. See also Movies S6 and S7.

Hoxb8-IRES-Cre; PC::G5-tdT animals carrying two allelic copies of the reporter cassette (Movie S7). The mean ATP-evoked peak $\Delta F/F_0$ response in homozygous microglia processes was 195.8% ± 26.07% (n = 10 cells) and in somas it was 180.1% ± 29.13% (n = 10 cells) (Figure 7D), suggesting a substantial increase in GCaMP5G response. Thus, our data indicate that PC::G5-tdT affords a powerful approach to investigate, in subcellular detail, the dynamics of calcium signaling in microglia.

DISCUSSION

Genetically encoded calcium indicators have evolved to rival synthetic dyes in essentially all aspects of in vivo imaging (Chen et al., 2013), encouraging the generation of new experimental models to unlock the full potential of this technology. We have utilized GCaMP5G in a reporter cassette with features that substantially improve the currently available toolbox. Similar to the previously generated Ai38 reporter using the GCaMP3 GECI (Zariwala et al., 2012), high expression levels are achieved with the powerful CAG promoter and posttranscriptional WPRE stabilizing element, allowing PC::G5-tdT to be highly and specifically expressed in neuronal and glial lineages with Cre. GCaMP5G has a higher signal-to-noise ratio, a wider $\Delta F/F_0$ range, and lower baseline fluorescence compared with GCaMP3 (Akerboom et al., 2012).

Several benefits are mediated by the inclusion of tdTomato fluorescence protein. First, this bright additional marker permits easy detection of cells with low intracellular calcium levels, in which GCaMP5G fluoresces very dimly. Since many Cre lineages are detectable in young newborns with wide field fluorescence, tdTomato also facilitates identification of desirable genotypes and/or expression patterns, reducing animal management cost. Second, tdTomato emission could also be used to normalize the GCaMP5G signal for ratiometric and motion

correction calculations. To our knowledge, no green emission emanating from the tdTomato protein has been reliably documented to interfere with the GCaMP signal. Nonetheless, the entire IRES-tdTomato cassette is flanked with functional FRT sites, and we have removed this marker in a separate GCaMP5G reporter line, PC::G5, which affords maximum sensitivity of detection.

Although highly expressed, the GCaMP5G-IRES-tdTomato cassette does not seem to affect the properties of the reporter animal at the single-cell, network, or behavioral levels. Calcium sequestration and buffering is a legitimate concern in cells expressing the GCaMP indicator at high levels and may be the cause of apparently decreased viability in virus-infected clls (Zariwala et al., 2012). We have therefore conducted a series of experiments to address this issue in PC::G5-tdT animals. Both membrane properties and long-term potentiation at synapses between Schaffer collaterals and CA1 in the hippocampus are not markedly affected in these animals (Figure S7). To specifically assess the effect of GCaMP5G expression at the organismal level, we generated animals ubiquitously expressing the GCaMP5G indicator only, by germline recombination of the PC::G5 line, and measured their behavior. Neither allele segregation nor body weight was statistically different from the control animals. Reassuringly, no significant differences were detected in their behavior, indicating that the reporter cassette in these animals does not extensively affect the central nervous system or growth and qualifies these animals for use in complex neurobehavioral experiments.

Of particular interest is the fact that PC::G5-tdT strongly and consistently reports intracellular calcium signaling in glia, which have been poorly accessible to specific monitoring of cell activity in vivo. The complexity of calcium transients within astrocyte processes is being unraveled, and our data corroborate some recent findings (Shigetomi et al., 2013). We show that monitoring of intracellular calcium in microglia is possible with endogenous reporters. Moreover, we demonstrate that, as in astrocytes, independent waves of activity can be visualized propagating through microglia processes and bulbous endings. Integration of these tools will allow researchers to directly interrogate microglial responses to sudden changes in brain physiology, including injury, inflammation, or abnormal neural activity.

We present a convenient locus, an intergenic region outside *Polr2a,* for inserting GECIs. This allows for scaling up GCaMP expression by increasing zygosity and gene dosage (unlike *ROSA26*, homozygous PC::G5-tdT mice have an intact transcriptome and high fertility) and by crossing with other strains harboring similar tools in other loci. If specific pairs of loxP sites are used in each site, incompatible between different loci, undesirable recombination can be prevented. More sensitive and faster probes such as GCaMP6S, GCaMP6M, and GCaMP6F (Chen et al., 2013) will be utilized in the next series of these reporter animals, with specific intracellular localizations. New lines with high-performance red-shifted GECIs are also highly desirable. Finally, site-specific recombinases such as Dre should be exploited to define parallel cell lineages to Cre for complex genetic experiments. Together, these efforts will enable previously inaccessible functional studies of brain physiology.

EXPERIMENTAL PROCEDURES

PC::G5-tdT Generation and Mouse Lines Used in This Study

The targeting vector shown in Figure 1A was prepared with DNA isolated from a lambda FIX II mouse 129/SV genomic library (Stratagene). A total of 8.5 kb of DNA homology harboring the last four exons of the *Polr2a* gene was subcloned into a pBluescript derivative using standard molecular cloning techniques. The reporter cassette, containing a CAG promoter (Niwa et al., 1991), GCaMP5G indicator (Addgene Plasmid No. 31788), IRES, tdTomato gene, WPRE element, and piggyBac ITRs was inserted in between PacI and EcoRI sites in the genomic clone, about 1 kb 3′ of the last exon of *Polr2a*. Premature expression of the reporter in the absence of Cre is prevented by several poly(A) signals in the loxP-flanked STOP cassette, also containing the neo selection marker in the opposite orientation. The targeting vector was linearized with AsiSI and electroporated into G4 ES cells of 129/C57Bl/6 hybrid background. Following selection with G418, two correctly targeted ES clones identified by southern blotting (Tvrdik and Capecchi, 2006) were expanded and injected into C57Bl/6 blastocysts for chimera generation. Positive offspring backcrossed to C57Bl/6 were bred to homozygosity. An alternative line, in which the IRES-tdTomato reporter has been deleted, was generated by breeding the PC::G5-tdT mice with a FLPe deleter (Rodríguez et al., 2000). This PC::G5 line expresses only GCaMP5G in Cre-positive cell lineages. For genotyping, four standard PCR primers have been designed. WT_FW 5′-GGC CTAATTGCTGAACCATC-3′ and WT_REV 5′-CTGGTGTATGCTGGAAATT GAA-3′ amplify a 360 bp wild-type product spanning the insertion site 3′ of *Polr2a*; Tg(GCaMP)_FW 5′- GCTGCTGCCCGACAACCACTAC-3′ and Tg(GCaMP)_REV 5′- CCTTCAGCTCGATGCGGTTCA-3′ amplify a 538 bp transgenic (GCaMP5G) product. Automated genotyping service for this strain is available from Transnetyx (Cordova, TN) using real-time PCR with specific probes designed for this locus ("Polr2a-3 WT," "GCaMP3-1 Tg," and/or "tdRFP").

We used the following Cre drivers to characterize the PC::G5-tdT reporter: *Emx1-IRES-Cre* (Gorski et al., 2002), *Cck-IRES-Cre* (Taniguchi et al., 2011), *CamKIIα-Cre* (Tsien et al., 1996), *GFAP-CreER* (Chow et al., 2008), and *Hoxb8-IRES-Cre* (Chen et al., 2010). Cre recombination in *GFAP-CreER* crosses was induced by intraperitoneal injections of 2–9 mg of tamoxifen in peanut oil per 40 g body weight. Germline recombination of PC::G5 was achieved with the *HPRT-Cre* line (Tang et al., 2002). All animal experiments carried out in this study were reviewed and approved by the University of Utah IACUC committee.

Immunohistochemistry and Confocal Imaging

Mice were anesthetized with Avertin (250 mg/kg body weight) and transcardially perfused with 4% formaldehyde (EMS 15713) in 1× PBS (pH 7.6). The brains were dissected, postfixed for 2 hr at room temperature, and processed through 10% sucrose in PBS overnight followed by 30% sucrose in PBS until they sink. These cryoprotected brains were embedded in 2% gelatin (Sigma G2500) and 0.9% NaCl in a metal mold, quickly frozen on a metal block cooled with liquid nitrogen, sectioned with Leica CM1900 at 20 μm thickness, and mounted on SuperFrost Gold Plus microscopy slides (Fisher Scientific). The sections were incubated with primary antibodies, chicken anti-GFP (Aves GFP-1020), rabbit anti-RFP (Rockland 600-401-379), and mouse anti-Cre Recombinase, Clone 2D8 (Millipore MAB3120), diluted in Cyto-Q Immuno Diluent and Block (Innovex Biosciences). The secondary antibodies were anti-chicken AF488, anti-rabbit AF555, and anti-mouse AF647, all made in goat (Life Technologies A11039, A21428, and A21235, respectively). The slides were stained with DAPI and mounted with Fluoromount-G (Southern Biotech), and image acquisition was performed with a Leica TCS SP5 confocal microscope. The images were analyzed and processed with Imaris 7.6.5 (Bitplane).

In Vivo Epifluorescence Imaging

Widefield epifluorescence imaging followed previously established protocols (Bozza et al., 2004; Spors et al., 2006; Wachowiak and Cohen, 2001). Awake P2 *Emx1-IRES-Cre*; PC::G5-tdT pups (n = 4) with skin and bone intact were gently restrained for 5–20 min and imaged on an Olympus BX51 illumination turret using an Olympus 4× 0.28 NA objective, a filter set optimized

for GFP (excitation: HQ480/40, dichroic: Q505LP, emission: HQ525/50; Semrock, Rochester, NY) and a 470 nm LED light source (Thorlabs, Newton, NJ) or 150W Xenon arc lamp (Opti-Quip, Highland Mills, NY). The light source power was attenuated using neutral density filters. The 256×256 pixel images were captured with a back-illuminated CCD camera (NeuroCCD SM-256; Red Shirt Imaging, Decatur, GA) at a frame rate of 25 Hz, digitized to 14 bit resolution and stored to the disk using Neuroplex software (Red Shirt Imaging).

In Vivo Two-Photon Imaging of Olfactory Bulb and Visual Cortex

For live imaging in the olfactory bulb, the mice were prepared using previously described methods (Wachowiak et al., 2013). Under pentobarbital (50 mg/kg) anesthesia, a double tracheotomy was performed and an artificial inhalation paradigm used. Animals were secured in a custom head holder for imaging, and at this point, isoflurane (0.5%–2% in O_2) was delivered directly to the lower tracheotomy tube, bypassing the nasal cavity. Body temperature and heart rate were maintained at 37°C and ~400 beats/min. A craniotomy covering half of the dorsal surface of the olfactory bulb was performed, filled with 2.5% low-melting point agarose in Ringer's solution and covered with a glass coverslip. Imaging was carried out with a two-photon microscope (MOM; Sutter Instruments) coupled to a pulsed Ti:Sapphire laser (Mai Tai HP; Spectra-Physics) and controlled by ScanImage 3.7 (Pologruto et al., 2003). Imaging was performed through a 20× 0.95 NA objective, and emitted light was collected by multialkali photomultiplier tubes (Hamamatsu R6357). A custom-built flow dilution olfactometer under computer control was used to deliver odorants. Odorants were presented for 4 s to the upper tracheotomy tube. The concentration of odorants ranged from 0.1% to 2% saturated vapor. Fluorescence time series were extracted and analyzed with custom MATLAB scripts. Fluorescence time series were converted to $\Delta F/F_0$ according to $\Delta F/F_0 = (F - F_0)/F_0$, where F_0 is the mean fluorescence over each trial. Pseudocolor glomerular-level activation maps reflect single trials in which movies were spatially filtered using a Gaussian window with a standard deviation of 1.25 pixels. Live imaging in the adult visual cortex was done under isoflurane anesthesia with a Prairie Technologies (Middleton, WI) imaging system using a 20× NA 0.95 Olympus lens.

Acute Brain Slice Preparation

Unless otherwise noted, 4- to 8-week-old male and female mice were used for acute brain slice experiments. The mice were anesthetized in a closed chamber with isoflurane (1.5%) and decapitated. The brains were rapidly removed and immersed in ice-cold cutting solution that contained 230 mM sucrose, 1 mM KCl, 0.5 mM $CaCl_2$, 10 mM $MgSO_4$, 26 mM $NaHCO_3$, 1.25 mM NaH_2PO_4, 0.04 mM Na-Ascorbate, and 10 mM glucose (pH = 7.2–7.4). Coronal slices (400 μm) were cut using a VT1200 vibratome (Leica Microsystems, Germany) and transferred to oxygenated aCSF that contained 124 mM NaCl, 2.5 mM KCl, 2 mM $CaCl_2$, 2 mM $MgSO_4$, 26 mM $NaHCO_3$, 1.25 mM NaH2PO_4, and 10 mM glucose (pH = 7.2–7.4; osmolarity = 310 mOsm). Slices were allowed to recover in oxygenated aCSF at room temperature for 1 hr before experiments. During the recordings, the slices were placed in a perfusion chamber and superfused with aCSF gassed with 95% O_2 and 5% CO_2 at 30°C–32°C for the duration of the experiment. Cells were visualized with a 20× water-immersion objective (Olympus Optical, New York, NY) and an IR1000 infrared CCD Monochrome Video Camera (Dage-MTI, Michigan City, IN).

Whole Cell Patch Clamp Electrophysiology

Electrodes were drawn on a horizontal puller (P97; Sutter Instruments, Novato, CA) using a filamented, thin-wall glass (World Precision Instruments, Sarasota, FL) and filled with an intracellular solution consisting of 120 mM K-gluconate, 20 mM KCl, 10 mM HEPES, 7 mM diTrisPhCr, 4 mM Na_2ATP, 2 mM $MgCl_2$, and 0.3 mM Tris-GTP and buffered to pH 7.3 with KOH. Final electrode resistances were between 2 and 5 MΩ, with access resistance values between 10 and 25 MΩ. Bridge balance compensation was used for all recording, and seal resistances were always greater than 1 GΩ. Electrophysiological recordings were performed with a current-clamp amplifier (Axoclamp 700A; Molecular Devices, Union City, CA) and filtered at 5 KHz and then digitized at 20 KHz using a Digidata 1550 (Molecular Devices, Union City, CA). Data were recorded using pClamp (Molecular Devices, Union City, CA). Individual spikes were identified using simple voltage threshold criteria (>0 mV). Spike frequency was then calculated as the number of spikes generated over a 500 ms long depolarization step elicited with DC current.

Ex Vivo Two-Photon Microscopy

Two-photon imaging was performed using a custom-built two-photon microscope (Lillis et al., 2008) built around a mode-locked Ti:Sapphire laser source emitting 140 fs pulses at an 80 MHz repetition rate with a wavelength adjustable from 690 to 1040 nm (Chameleon Ultra I; Coherent, Santa Clara, CA). We primarily used laser emission wavelengths of 930 nm to excite GCaMP5G or 1040 nm to excite tdTomato. In this setup, laser power is attenuated using an electro-optic modulator (ConOptics, Danbury, CT), and scanning is accomplished using x-y galvanometer-mounted mirrors (GSI Lumonics, Billerica, MA) controlled by custom LabVIEW software and a PCI-6221 data acquisition board (National Instruments, Austin, TX). Full field of view images were acquired with XY raster scanning. We used a 20× 0.95 NA water-immersion objective (Olympus, Tokyo, Japan). Emitted photons were bandpass filtered (Semrock, Rochester, NY) at (peak/bandwidth) 525/50 nm (GCaMP5G) and 593/46 nm (tdTomato) and collected by a wide band (300–650 nm) and low noise photomultiplier tube (H7360-01; Hamamatsu, Hamamatsu City, Japan). Changes in fluorescence (ΔF) were quantified using ImageJ (NIH) software and expressed as a percentage of baseline (% $\Delta F/F_0$). Time-lapse images of astrocyte and microglia calcium signaling were recorded at a frame rate of 1 Hz. ROIs were selected based on the appearance of GCaMP5G calcium transients in the time-lapse images. Spontaneous calcium transients in astrocyte somas and processes were defined as an event when changes in GCaMP5G $\Delta F/F_0$ increased 2 standard deviations (σ) above baseline. To trigger calcium elevations, agonists were dissolved in aCSF and delivered locally by a pressure pulse (10 psi; 100 ms) using a Picospritzer III (Parker Instrumentation, Chicago, IL).

In Vivo Recording in Barrel Cortex and Calcium Imaging

Animal preparation was modified from a previously described method (Wang et al., 2006). Briefly, adult mice (5 to 8 weeks old) were anesthetized with ketamine (80–100 mg/kg) and xylazine (8–10 mg/kg). Body temperature was monitored using a rectal probe and maintained with a heating blanket. Vitals were monitored throughout the experiment using a pulse oximeter and heart rate monitor (Kent Scientific, Torrington, CT). A custom-built stainless steel frame with a 3 mm opening was glued over the right somatosensory cortex. A 1–2 mm craniotomy was then performed, and the dura was carefully removed. The opening was filled with 1% agarose (wt/vol) and covered with a glass coverslip. The animal was placed on a stage and the head restrained during imaging. Time series images of astrocyte calcium increases were recorded at 1 Hz using custom LabVIEW software and the custom-built two-photon laser scanning setup described in the previous section.

Whisker Stimulation

Whisker stimulation was delivered as previously described with modifications (Wang et al., 2006). Briefly, puffs of compressed air were delivered using a PicoSpritzer III (Parker Instrumentation, Chicago, IL) and pClamp Software (Molecular Devices, Union City, CA). Stimuli consisted of 100 ms air puffs delivered at 5 Hz for 30 s with a 5 s delay at onset.

Statistical Analysis

Unless otherwise stated, all results are reported as mean ± SEM, and statistical tests were deemed significant when $p < 0.05$. Statistical calculations were performed either with MATLAB (MathWorks, Natick, MA) or GraphPad Prism 6.0 (GraphPad Software, La Jolla, CA).

SUPPLEMENTAL INFORMATION

Supplemental Information includes Supplemental Experimental Procedures, seven figures, and seven movies and can be found with this article online at http://dx.doi.org/10.1016/j.neuron.2014.07.024.

ACKNOWLEDGMENTS

We thank Lara Carroll and Sen Wu for sharing useful plasmid constructs, Carol Lenz and Sheila Barnett for ES cell culture work, and Richard Focht and Jim Hayes for blastocyst injections and embryo implantations. We also thank Karl Lustig, June Wangerin, and E. Jill Dahle for assistance with mouse husbandry. We are grateful to Mark Geyer and his lab for providing PPI protocols and SR-Lab training and Kyle Lillis for technical assistance. The GCaMP5G plasmid, acquired from Addgene, was kindly deposited by Loren Looger. This work was supported by the Epilepsy Foundation Predoctoral Research Training Fellowship (J.M.G.), the University of Utah Seed Grant Program (P.T., K.S.W., J.A.W., and M.R.C.), NIH K99/R00 NS076364 (J.D.S.), NIH R21 OD016562 (P.T.), NIH R03 MH103728, the Ben B. and Iris M. Margolis Foundation Award (K.S.W. and J.A.W.), and NIH RC1 NS069033 and NIH R01 NS078331 (K.S.W. and J.A.W.).

Accepted: July 17, 2014
Published: August 21, 2014

REFERENCES

Adelsberger, H., Garaschuk, O., and Konnerth, A. (2005). Cortical calcium waves in resting newborn mice. Nat. Neurosci. *8*, 988–990.

Akerboom, J., Chen, T.W., Wardill, T.J., Tian, L., Marvin, J.S., Mutlu, S., Calderon, N.C., Esposti, F., Borghuis, B.G., Sun, X.R., et al. (2012). Optimization of a GCaMP calcium indicator for neural activity imaging. J. Neurosci. *32*, 13819–13840.

Anderson, C.M., and Swanson, R.A. (2000). Astrocyte glutamate transport: review of properties, regulation, and physiological functions. Glia *32*, 1–14.

Ballabh, P., Braun, A., and Nedergaard, M. (2004). The blood-brain barrier: an overview: structure, regulation, and clinical implications. Neurobiol. Dis. *16*, 1–13.

Bozza, T., McGann, J.P., Mombaerts, P., and Wachowiak, M. (2004). In vivo imaging of neuronal activity by targeted expression of a genetically encoded probe in the mouse. Neuron *42*, 9–21.

Brancaccio, M., Maywood, E.S., Chesham, J.E., Loudon, A.S., and Hastings, M.H. (2013). A Gq-Ca2+ axis controls circuit-level encoding of circadian time in the suprachiasmatic nucleus. Neuron *78*, 714–728.

Brawek, B., Schwendele, B., Riester, K., Kohsaka, S., Lerdkrai, C., Liang, Y., and Garaschuk, O. (2014). Impairment of in vivo calcium signaling in amyloid plaque-associated microglia. Acta Neuropathol. *127*, 495–505.

Casper, K.B., and McCarthy, K.D. (2006). GFAP-positive progenitor cells produce neurons and oligodendrocytes throughout the CNS. Mol. Cell. Neurosci. *31*, 676–684.

Chen, S.K., Tvrdik, P., Peden, E., Cho, S., Wu, S., Spangrude, G., and Capecchi, M.R. (2010). Hematopoietic origin of pathological grooming in Hoxb8 mutant mice. Cell *141*, 775–785.

Chen, Q., Cichon, J., Wang, W., Qiu, L., Lee, S.J., Campbell, N.R., Destefino, N., Goard, M.J., Fu, Z., Yasuda, R., et al. (2012). Imaging neural activity using Thy1-GCaMP transgenic mice. Neuron *76*, 297–308.

Chen, T.W., Wardill, T.J., Sun, Y., Pulver, S.R., Renninger, S.L., Baohan, A., Schreiter, E.R., Kerr, R.A., Orger, M.B., Jayaraman, V., et al. (2013). Ultrasensitive fluorescent proteins for imaging neuronal activity. Nature *499*, 295–300.

Chow, L.M.L., Zhang, J., and Baker, S.J. (2008). Inducible Cre recombinase activity in mouse mature astrocytes and adult neural precursor cells. Transgenic Res. *17*, 919–928.

Cui, G., Jun, S.B., Jin, X., Pham, M.D., Vogel, S.S., Lovinger, D.M., and Costa, R.M. (2013). Concurrent activation of striatal direct and indirect pathways during action initiation. Nature *494*, 238–242.

Ding, F., O'Donnell, J., Thrane, A.S., Zeppenfeld, D., Kang, H., Xie, L., Wang, F., and Nedergaard, M. (2013). α1-Adrenergic receptors mediate coordinated Ca2+ signaling of cortical astrocytes in awake, behaving mice. Cell Calcium *54*, 387–394.

Doetsch, F., Caillé, I., Lim, D.A., García-Verdugo, J.M., and Alvarez-Buylla, A. (1999). Subventricular zone astrocytes are neural stem cells in the adult mammalian brain. Cell *97*, 703–716.

Eichhoff, G., Brawek, B., and Garaschuk, O. (2011). Microglial calcium signal acts as a rapid sensor of single neuron damage in vivo. Biochim. Biophys. Acta *1813*, 1014–1024.

Garcia, A.D., Doan, N.B., Imura, T., Bush, T.G., and Sofroniew, M.V. (2004). GFAP-expressing progenitors are the principal source of constitutive neurogenesis in adult mouse forebrain. Nat. Neurosci. *7*, 1233–1241.

Gorski, J.A., Talley, T., Qiu, M., Puelles, L., Rubenstein, J.L.R., and Jones, K.R. (2002). Cortical excitatory neurons and glia, but not GABAergic neurons, are produced in the Emx1-expressing lineage. J. Neurosci. *22*, 6309–6314.

Haustein, M.D., Kracun, S., Lu, X.H., Shih, T., Jackson-Weaver, O., Tong, X., Xu, J., Yang, X.W., O'Dell, T.J., Marvin, J.S., et al. (2014). Conditions and constraints for astrocyte calcium signaling in the hippocampal mossy fiber pathway. Neuron *82*, 413–429.

Haydon, P.G. (2001). GLIA: listening and talking to the synapse. Nat. Rev. Neurosci. *2*, 185–193.

Hickman, S.E., Kingery, N.D., Ohsumi, T.K., Borowsky, M.L., Wang, L.C., Means, T.K., and El Khoury, J. (2013). The microglial sensome revealed by direct RNA sequencing. Nat. Neurosci. *16*, 1896–1905.

Joshi, P.S., Molyneaux, B.J., Feng, L., Xie, X., Macklis, J.D., and Gan, L. (2008). Bhlhb5 regulates the postmitotic acquisition of area identities in layers II-V of the developing neocortex. Neuron *60*, 258–272.

Kato, H.K., Chu, M.W., Isaacson, J.S., and Komiyama, T. (2012). Dynamic sensory representations in the olfactory bulb: modulation by wakefulness and experience. Neuron *76*, 962–975.

Laywell, E.D., Rakic, P., Kukekov, V.G., Holland, E.C., and Steindler, D.A. (2000). Identification of a multipotent astrocytic stem cell in the immature and adult mouse brain. Proc. Natl. Acad. Sci. USA *97*, 13883–13888.

Lillis, K.P., Eng, A., White, J.A., and Mertz, J. (2008). Two-photon imaging of spatially extended neuronal network dynamics with high temporal resolution. J. Neurosci. Methods *172*, 178–184.

Madisen, L., Zwingman, T.A., Sunkin, S.M., Oh, S.W., Zariwala, H.A., Gu, H., Ng, L.L., Palmiter, R.D., Hawrylycz, M.J., Jones, A.R., et al. (2010). A robust and high-throughput Cre reporting and characterization system for the whole mouse brain. Nat. Neurosci. *13*, 133–140.

Nakai, J., Ohkura, M., and Imoto, K. (2001). A high signal-to-noise Ca(2+) probe composed of a single green fluorescent protein. Nat. Biotechnol. *19*, 137–141.

Namiki, S., Norimoto, H., Kobayashi, C., Nakatani, K., Matsuki, N., and Ikegaya, Y. (2013). Layer III neurons control synchronized waves in the immature cerebral cortex. J. Neurosci. *33*, 987–1001.

Nedergaard, M., Ransom, B., and Goldman, S.A. (2003). New roles for astrocytes: redefining the functional architecture of the brain. Trends Neurosci. *26*, 523–530.

Niwa, H., Yamamura, K., and Miyazaki, J. (1991). Efficient selection for high-expression transfectants with a novel eukaryotic vector. Gene *108*, 193–199.

Pologruto, T.A., Sabatini, B.L., and Svoboda, K. (2003). ScanImage: flexible software for operating laser scanning microscopes. Biomed. Eng. Online *2*, 13.

Powell, S.B., Zhou, X., and Geyer, M.A. (2009). Prepulse inhibition and genetic mouse models of schizophrenia. Behav. Brain Res. *204*, 282–294.

Rodríguez, C.I., Buchholz, F., Galloway, J., Sequerra, R., Kasper, J., Ayala, R., Stewart, A.F., and Dymecki, S.M. (2000). High-efficiency deleter mice show that FLPe is an alternative to Cre-loxP. Nat. Genet. *25*, 139–140.

Seri, B., García-Verdugo, J.M., McEwen, B.S., and Alvarez-Buylla, A. (2001). Astrocytes give rise to new neurons in the adult mammalian hippocampus. J. Neurosci. *21*, 7153–7160.

Seroogy, K.B., Brecha, N., and Gall, C. (1985). Distribution of cholecystokinin-like immunoreactivity in the rat main olfactory bulb. J. Comp. Neurol. *239*, 373–383.

Shigetomi, E., Bushong, E.A., Haustein, M.D., Tong, X., Jackson-Weaver, O., Kracun, S., Xu, J., Sofroniew, M.V., Ellisman, M.H., and Khakh, B.S. (2013). Imaging calcium microdomains within entire astrocyte territories and endfeet with GCaMPs expressed using adeno-associated viruses. J. Gen. Physiol. *141*, 633–647.

Spors, H., Wachowiak, M., Cohen, L.B., and Friedrich, R.W. (2006). Temporal dynamics and latency patterns of receptor neuron input to the olfactory bulb. J. Neurosci. *26*, 1247–1259.

Tang, S.-H.E., Silva, F.J., Tsark, W.M.K., and Mann, J.R. (2002). A Cre/loxP-deleter transgenic line in mouse strain 129S1/SvImJ. Genesis *32*, 199–202.

Taniguchi, H., He, M., Wu, P., Kim, S., Paik, R., Sugino, K., Kvitsiani, D., Fu, Y., Lu, J., Lin, Y., et al. (2011). A resource of Cre driver lines for genetic targeting of GABAergic neurons in cerebral cortex. Neuron *71*, 995–1013.

Thrane, A.S., Rangroo Thrane, V., Zeppenfeld, D., Lou, N., Xu, Q., Nagelhus, E.A., and Nedergaard, M. (2012). General anesthesia selectively disrupts astrocyte calcium signaling in the awake mouse cortex. Proc. Natl. Acad. Sci. USA *109*, 18974–18979.

Tian, L., Hires, S.A., Mao, T., Huber, D., Chiappe, M.E., Chalasani, S.H., Petreanu, L., Akerboom, J., McKinney, S.A., Schreiter, E.R., et al. (2009). Imaging neural activity in worms, flies and mice with improved GCaMP calcium indicators. Nat. Methods *6*, 875–881.

Tsien, J.Z., Chen, D.F., Gerber, D., Tom, C., Mercer, E.H., Anderson, D.J., Mayford, M., Kandel, E.R., and Tonegawa, S. (1996). Subregion- and cell type-restricted gene knockout in mouse brain. Cell *87*, 1317–1326.

Tvrdik, P., and Capecchi, M.R. (2006). Reversal of Hox1 gene subfunctionalization in the mouse. Dev. Cell *11*, 239–250.

Wachowiak, M., and Cohen, L.B. (2001). Representation of odorants by receptor neuron input to the mouse olfactory bulb. Neuron *32*, 723–735.

Wachowiak, M., Economo, M.N., Díaz-Quesada, M., Brunert, D., Wesson, D.W., White, J.A., and Rothermel, M. (2013). Optical dissection of odor information processing in vivo using GCaMPs expressed in specified cell types of the olfactory bulb. J. Neurosci. *33*, 5285–5300.

Wang, X., Lou, N., Xu, Q., Tian, G.F., Peng, W.G., Han, X., Kang, J., Takano, T., and Nedergaard, M. (2006). Astrocytic Ca2+ signaling evoked by sensory stimulation in vivo. Nat. Neurosci. *9*, 816–823.

Wang, F., Smith, N.A., Xu, Q., Fujita, T., Baba, A., Matsuda, T., Takano, T., Bekar, L., and Nedergaard, M. (2012). Astrocytes modulate neural network activity by Ca^{2}+-dependent uptake of extracellular K+. Sci. Signal. *5*, ra26.

West, P.J., Saunders, G.W., Remigio, G.J., Wilcox, K.S., and White, H.S. (2014). Antiseizure drugs differentially modulate θ-burst induced long-term potentiation in C57BL/6 mice. Epilepsia *55*, 214–223.

Yonehara, K., Farrow, K., Ghanem, A., Hillier, D., Balint, K., Teixeira, M., Jüttner, J., Noda, M., Neve, R.L., Conzelmann, K.K., and Roska, B. (2013). The first stage of cardinal direction selectivity is localized to the dendrites of retinal ganglion cells. Neuron *79*, 1078–1085.

Zariwala, H.A., Borghuis, B.G., Hoogland, T.M., Madisen, L., Tian, L., De Zeeuw, C.I., Zeng, H., Looger, L.L., Svoboda, K., and Chen, T.W. (2012). A Cre-dependent GCaMP3 reporter mouse for neuronal imaging in vivo. J. Neurosci. *32*, 3131–3141.